

# Elucidation of Functional Groups on Gram-Positive and Gram-Negative Bacterial Surfaces Using Infrared Spectroscopy

Wei Jiang,<sup>\*,†</sup> Anuradha Saxena,<sup>‡</sup> Bongkeun Song,<sup>†</sup> Bess B. Ward,<sup>†</sup>  
Terry J. Beveridge,<sup>‡</sup> and Satish C. B. Myneni<sup>†,§</sup>

*Department of Geosciences, Princeton University, Princeton, New Jersey 08544, Department of Microbiology, University of Guelph, Guelph, Canada, and Earth Sciences Division, Lawrence Berkeley National Laboratory, Berkeley, California 94720*

*Received April 15, 2004. In Final Form: August 19, 2004*

Surface functional group chemistry of intact Gram-positive and Gram-negative bacterial cells and their isolated cell walls was examined as a function of pH, growth phase, and growth media (for intact cells only) using attenuated total reflectance Fourier transform infrared (ATR-FTIR) spectroscopy. Infrared spectra of aqueous model organic molecules, representatives of the common functional groups found in bacterial cell walls (i.e., hydroxyl, carboxyl, phosphoryl, and amide groups), were also examined in order to assist the interpretation of the infrared spectra of bacterial samples. The surface sensitivity of the ATR-FTIR spectroscopic technique was evaluated using diatom cells, which possess a several-nanometers-thick layer of glycoprotein on their silica shells. The ATR-FTIR spectra of bacterial surfaces exhibit carboxyl, amide, phosphate, and carbohydrate related features, and these are identical for both Gram-positive and Gram-negative cells. These results provide direct evidence to the previously held conviction that the negative charge of bacterial surfaces is derived from the deprotonation of both carboxylates and phosphates. Variation in solution pH has only a minor effect on the secondary structure of the cell wall proteins. The cell surface functional group chemistry is altered neither by the growth phase nor by the growth medium of bacteria. This study reveals the universality of the functional group chemistry of bacterial cell surfaces.

## 1. Introduction

Bacteria are ubiquitous in near-surface geological systems, and are known to play important role in different biogeochemical processes, including contaminant transport and degradation,<sup>1,2</sup> mineral dissolution and precipitation,<sup>3</sup> and metal sorption by minerals and their redox transformations.<sup>4–9</sup> Bacteria–water interfacial chemistry is one of the critical variables that play a central role in mediating these bacterial reactions. In addition, bacterial transport through porous media, adhesion to minerals and biological tissue, response to antibiotics, and the formation and chemistry of biofilms are also modified by the bacterial surface chemistry.<sup>10–14</sup> The composition and structure of bacterial cell walls, and their variation as a

function of different environmental variables (e.g., pH, solution and substrate composition), is responsible for most surface interactions of bacteria. While the bulk chemical composition of bacterial cell walls is often known, their ability to complex metals and attach to surfaces as a function of different environmental conditions is not well understood.

The Gram-positive cell wall is primarily made up of peptidoglycan (ca. 40–80% of the dry weight of the wall), which is a polymer of *N*-acetylglucosamine and *N*-acetylmuramic acid, containing mainly carboxyl, amide, and hydroxyl functional groups.<sup>15</sup> The two other important constituents of Gram-positive cell walls are teichoic acid, a polymer of glycopyranosyl glycerol phosphate, and teichuronic acid, which is similar to teichoic acid, but replaces the phosphate functional groups with carboxyls. The cell walls of Gram-negative bacteria are more complex due to the presence of an outer membrane in addition to a thin peptidoglycan layer, but do not contain teichoic or teichuronic acids.<sup>16</sup> Instead, the outer membrane contains phospholipids, lipoproteins, lipopolysaccharides, and proteins.

Several recent investigations examined the surface chemistry of intact bacterial cells and their cell walls using both macroscopic (e.g., potentiometric titration, ion adsorption) and molecular tools (microscopy and

\* Corresponding author. Telephone: (609) 258-3827. E-mail: wjiang@princeton.edu.

<sup>†</sup> Princeton University.

<sup>‡</sup> University of Guelph.

<sup>§</sup> Lawrence Berkeley National Laboratory.

(1) Corapcioglu, M. Y.; Kims. *Water Resour. Res.* **1995**, *31*, 2639–2648.

(2) Watanabe, K.; Hamamura, N. *Curr. Opin. Biotechnol.* **2003**, *14*, 289–295.

(3) Stillings, L. L.; Drever, J. I.; Brantley, S. L.; Sun, Y.; Oxburgh, R. *Chem. Geol.* **1996**, *132*, 79–90.

(4) Beveridge, T. J.; Forsberg, C. W.; Doyle, R. J. *J. Bacteriol.* **1982**, *150*, 1438–1448.

(5) Suzuki, T.; Miyata, H.; Kawai, K.; Takmizawa, K.; Tai, Y.; Okazaki, M. *J. Bacteriol.* **1992**, *174*, 5340–5345.

(6) Jackson, T. A.; West, M. M.; Leppard, G. G. *Environ. Sci. Technol.* **1999**, *33*, 3795–3801.

(7) Holman, H. N.; Perry, D. L.; Martin, M. C.; Lamble, G. M.; McKinney, W. R.; Hunter-Cevera, J. C. *Geomicrobiol. J.* **1999**, *16*, 307–324.

(8) Klaus-Joerger, T.; Joerger, R.; Olsson, E.; Granqvist, C. G. *Trends Biotechnol.* **2001**, *19*, 15–20.

(9) Fein, J. B.; Fowle, D. A.; Cahill, J.; Kemner, K.; Boyanov, M.; Bunker, B. *Geomicrobiol. J.* **2002**, *19*, 369–382.

(10) McWhirter, M. J.; Bremer, P. J.; Lamont, I. L.; McQuillan, A. *J. Langmuir* **2003**, *19*, 3575–3577.

(11) Burdman, S.; Okon, Y.; Jurkevitch, E. *Crit. Rev. Microbiol.* **2000**, *26*, 91–110.

(12) Nelson, Y. M.; Lion, L. W.; Shuler, M. L.; Ghiorso, W. C. *Environ. Sci. Technol.* **1996**, *30*, 2027–2035.

(13) Decho, A. W. *Continental Shelf Res.* **2000**, *20*, 1257–1273.

(14) Suci, P. A.; Geesey, G. G.; Tyler, B. J. *J. Microbiol. Methods* **2001**, *46*, 193–208.

(15) Beveridge, T. J. *Int. Rev. Cytol.* **1981**, *72*, 229–317.

(16) Perry, J. J.; Staley, J. T.; Lory, S. *Microbial Life*; Sinauer Associates, Inc.: Sunderland, MA, 2002; pp 61–100.

spectroscopy).<sup>17–26</sup> This research led to the identification of major proton-active functional groups on bacterial surfaces and the development of a series of thermodynamic metal binding constants for them.<sup>27–30</sup> However, molecular information to support the loci of protonation and complexation remains limited. Structural probes, such as transmission and scanning electron microscopes, are often used to study microbial cell surfaces.<sup>31,32</sup> These methods require subjecting the specimen to high vacuum, thereby affecting natural hydration levels of the biopolymers, and possibly altering the cell morphological characteristics. The cells are also susceptible to alterations in the presence of the high energy of the electron beam. Although cryogenic techniques can alleviate this problem over short exposure periods, the cell structure can be altered during sample freezing if a vitreous state is not rapidly achieved. In addition, the electron microscopic methods cannot provide in situ information on the functional group characteristics of cell walls. More recently, researchers have begun using in situ methods, such as infrared and Raman spectroscopies, to study the behavior of bacteria–water interfaces, and their interactions with various chemicals.<sup>33–35</sup> While these studies have shown the dominant vibrational modes of lipopolysaccharide, phospholipids, and protein components in the cell wall, identification of different functional groups from the infrared spectra and their variation as a function of solution composition is still not complete.<sup>35,36</sup> Researchers also argue that isolated cell envelopes may not provide complete information on intact bacterial cells, since the chemical environment of the cell wall is significantly altered during the isolation process and in addition it is not adjacent to an energized membrane.<sup>37</sup>

The objective of our research was to obtain functional group specific information on bacterial surfaces in aqueous solutions, and to observe their variation as a function of cell structure (Gram-positive versus Gram-negative cells) and solution composition. Attenuated total reflectance Fourier transform infrared (ATR-FTIR) spectroscopy was used to examine these interfacial properties of cells. To assist the interpretation of spectral features of bacterial cells, small chain organic molecules of known structure and functional groups, similar to those found in bacterial cell walls, were also examined. This is important to establish the sensitivity of ATR-FTIR spectra in the unequivocal identification of different functional groups and their changes with pH. Since it has been shown that surface reactivity of bacterial cells depends on the metabolic state of cells (active, inactive, or dead),<sup>38</sup> experiments were also conducted to evaluate the variations in cell wall chemistry as a function of growth stage and growth medium. Cell walls were also isolated from both Gram-positive and Gram-negative cells to help evaluate the sensitivity of the technique to differences in surfaces of bacteria.

**Sensitivity of ATR-FTIR to Bacterial Surfaces.** In ATR-FTIR spectroscopy, the infrared beam is allowed to go through the ATR crystal and to be totally reflected at the ATR crystal–sample interface. An evanescent wave, generated at the reflecting surface, penetrates the rarer medium. This wave has the same frequency as that of the incident photons, while its amplitude decreases exponentially away from the interface according to the equation

$$E = E_0 e^{-Z/d_p} \quad (1)$$

where  $E_0$  and  $E$  are the electric field amplitudes at the interface and at a depth  $Z$  away from the interface, respectively, and  $d_p$  is the penetration depth, defined as the  $e^{-1}$  depth.  $d_p$  is given by

$$d_p = \frac{\lambda}{2\pi(n_c^2 \sin^2 \theta - n_s^2)^{1/2}} \quad (2)$$

where  $\theta$  is the angle of incidence,  $\lambda$  is the wavelength of the infrared radiation, and  $n_s$  and  $n_c$  are refractive indices of sample and the ATR crystal, respectively. For example, the penetration depth for bacterial cells ( $n_s \sim 1.39$ )<sup>41</sup> in contact with a Ge ATR crystal ( $n_c = 4.0$ ) that accepts the incident infrared beam at  $60^\circ$  is 339 nm at  $1000 \text{ cm}^{-1}$  and 188 nm at  $1800 \text{ cm}^{-1}$ . It should be noted that this is  $1/e$  depth, and the absolute penetration of the evanescent wave can be greater than these estimates. The refractive index of bacterial cells in the visible region is estimated to be around 1.39, and it is assumed that the refractive indices of bacterial cells in the infrared and visible regions are similar. Several small chain organic molecules are also reported to have refractive indices close to 1.40.<sup>42</sup> In addition, there are several other ATR crystals with lower refractive indices that accept an infrared beam at different

- (17) Schatten, G.; Pawley, J. B. *Science* **1988**, *239*, 164.  
 (18) Neidhardt, F. C.; Ingraham, J. L.; Schaecher, M. *Physiology of the bacterial cell: a molecular approach*; Sinauer Associates, Inc.: Sunderland, MA, 1990.  
 (19) Gerhardt, P. R.; Murray, G. E.; Wood, W. A.; Krieg, N. R. *Methods for general and molecular bacteriology*; American Society for Microbiology: Washington, DC, 1994; Vol. 4.  
 (20) Handrea, M.; Sahre, M.; Neubauer, A.; Sleytr, U. B.; Kautek, W. *Bioelectrochemistry* **2003**, *61*, 1–8.  
 (21) Schar-Zammaretti, P.; Ubbink, J. *Biophys. J.* **2003**, *85*, 4076–4092.  
 (22) Mullen, M. D.; Wolf, D. C.; Ferris, F. G.; Beveridge, T. J.; Flemming, C. A.; Bailey, G. W. *Appl. Environ. Microbiol.* **1989**, *55*, 3143–3149.  
 (23) Fein, J. B.; Daughney, C. J.; Yee, N.; Davis, T. *Geochim. Cosmochim. Acta* **1997**, *61*, 3319–3328.  
 (24) Fowle, D. A.; Fein, J. B. *Geochim. Cosmochim. Acta* **1999**, *63*, 3059–3067.  
 (25) Benning, L.; Phoenix, V. R.; Yee, N.; Konhauser, K. O. *Geochim. Cosmochim. Acta* **2004**, *68*, 743–757.  
 (26) Benning, L.; Phoenix, V. R.; Yee, N.; Tobin, M. J. *Geochim. Cosmochim. Acta* **2004**, *68*, 729–741.  
 (27) Beveridge, T. J.; Murray, R. G. E. *J. Bacteriol.* **1980**, *141*, 876–887.  
 (28) Beveridge, T. J.; Forsberg, C. W.; Doyle, R. J. *J. Bacteriol.* **1982**, *150*, 1438–1448.  
 (29) Small, T. D.; Warren, L. A.; Roden, E. E.; Ferris, F. G. *Environ. Sci. Technol.* **1999**, *33*, 4465–4470.  
 (30) Phoenix, V. R.; Martinez, R. E.; Konhauser, K. O.; Ferris, F. G. *Appl. Environ. Microbiol.* **2002**, *68*, 4827–4834.  
 (31) Wahl, R.; Raff, J.; Selenska-Pobell, S.; Mertig, M.; Pompe, W. *Biotechnol. Lett.* **2001**, *23*, 1485–1490.  
 (32) Erlandsen, S.; Lei, M.; Martin-Lacave, I.; Dunny, G.; Wells, C. *Microsc. Microanal.* **2003**, *9*, 273–278.  
 (33) Naumann, D.; Helm, D.; Labischinski, H. *Nature* **1991**, *351*, 81–82.  
 (34) Naumann, D.; Helm, D.; Labischinski, H.; Giesbrecht, P. In *Modern Techniques for Rapid Microbiological Analysis*; Nelson, W. H., Ed.; VCH: New York, 1991; p 43.  
 (35) Reiter, G.; Siam, M.; Falkenhagen, D.; Gollnertsch, W.; Baurecht, D.; Fringeli, U. P. *Langmuir* **2002**, *18*, 5761–5771.  
 (36) Kamnev, A. A.; Antonyuk, L. P.; Matora, L. Y.; Serebrennikova, O. B.; Sumaroka, M. V.; Colina, M.; Renou-Gonnord, M. F.; Ignatov, V. *J. Mol. Struct.* **1999**, *481*, 387–393.

(37) Urrutia, M. M. General bacterial sorption processes. In *Biosorbents for Metal Ions*; Wase, J., Forster, C., Eds.; Taylor and Francis: London, 1997; pp 39–66.

(38) Parmar, N.; Warren, L. A.; Roden, E. E.; Ferris, F. G. *Chem. Geol.* **2000**, *169*, 281–288.

(39) Ostergren, J. D.; Trainor, T. P.; Bargar, J. R.; Brown, G. E., Jr.; Parks, G. A. *J. Colloid Interface Sci.* **2000**, *225*, 466–482.

(40) Billingham, J.; Breen, C.; Yarwood, J. *Vib. Spectrosc.* **1997**, *14*, 19–34.

(41) Busalmen, J. P.; de Sanchez, S. R.; Schiffrin, D. *J. Appl. Environ. Microbiol.* **1998**, *64*, 3690–3697.

(42) Lide, D. R. *Handbook of chemistry and physics*, 75th ed.; CRC Press: Boca Raton, 1994.

incident angles. However, of all commercially available crystals, Ge crystal with a 60° incident angle gives the shallowest penetration depth. The average thickness of the bacterial cell wall ranges from 20 to 50 nm.<sup>15</sup> On the basis of the above calculations, it is apparent that the evanescent wave should penetrate the interior of the bacterial cells, provided they are attached to the ATR crystal surface.

It should be noted that there are uncertainties associated with these penetration depth estimates. When cell suspension is placed on the ATR crystal surface, some cells may be in direct contact with the crystal, while water film separates others. The penetration depth estimates shown above are valid for the cells in direct contact with the ATR crystal, while these estimates do not represent the cells that do not attach to the crystal. This is because the evanescent wave penetrates the cell through an intermediate water film of lower refractive index (when compared to the refractive index of the cell) and unknown thickness, and because of the uncertainty of the behavior of the wave at the water–cell wall interface. In addition, the uncertainty of refractive indices of the bacterial cell walls in the infrared region, and the macromolecular structure of its components (open versus condensed) and their variation with solution composition, may significantly alter the penetration depth estimates. Hence, an ATR-FTIR spectrum of bacterial suspension represents these sum effects, and the spectrum cannot be attributed to the surfaces alone. In this study, the ATR-FTIR spectra of live diatom cells, which contain a coating of a few nanometers of glycoprotein on their silica shells, and diatom cells without this organic casing, are used to estimate the penetration depth of the evanescent wave. In addition, spectral differences between the live intact cells and lysed cells were used to identify the surface sensitivity of the infrared spectroscopic technique.

## 2. Materials and Methods

**2.1. Model Molecules.** The chemicals used in this study were reagent grade or better, and they were obtained from Sigma-Aldrich. Model organic molecules selected for this investigation were d-glucuronic acid (sodium salt monohydrate), phytic acid (sodium salt), tripolyphosphate, and l-rhamnose (monohydrate). About 50 mM aqueous solutions of these compounds were prepared for obtaining their infrared spectra. Solution pH was adjusted between 2 and 10 using appropriate quantities of 0.1 M HCl and 0.1 M NaOH. Samples examined at extreme pH values (2 and 10) were back-titrated to pH 7 to ensure that the alteration of sample chemical structure during pH titration was absent. All solutions were prepared using deionized water.

**2.2. Bacterial Cell Cultures.** Bacterial species examined in this study were *Bacillus subtilis* 168, *Bacillus licheniformis*, *Pseudomonas stutzeri* 17588, and *Pseudomonas aeruginosa* PAO1. All these species were cultured in Tryptic Soy broth (TSB) medium for 24 h at 25 °C. *P. stutzeri* cells were in addition grown in Luria-Bertani (LB) broth medium to evaluate the influence of growth medium on the cell surface chemistry. The cells were removed from the nutrient medium by centrifugation, and rinsed three times with a 0.1 M NaNO<sub>3</sub> solution. The pH of each washed cell suspension was recorded. The suspensions were later centrifuged at 3300g for 10 min, and the cell pellets were transferred onto an ATR crystal surface for further analysis. Infrared spectra of the cells were collected using their supernatants for the spectral background. Additional cell suspensions with pH values between 2 and 10 were also prepared separately by adding appropriate quantities of 0.1 M HCl or 0.1 M NaOH to small quantities of washed cell suspensions. *P. stutzeri* cells were also analyzed at different growth stages. The growth stages were monitored using the optical density measurements of cell suspensions at a wavelength of 600 nm (OD<sub>600</sub>). These measurements were made using a Beckman DU530 UV/vis spectrophotometer. LB broth consisted of 10.0 g of tryptone, 5.0 g of yeast

extract, and 0.5 g of NaCl per liter of solution, whereas TSB consisted of 17.0 g of pancreatic digest of casein, 3.0 g of papaic digest of soybean meal, 2.5 g of dextrose, 5.0 g of NaCl, and 2.5 g of dipotassium phosphate in 1 L of solution. Lysed bacterial cell suspensions were prepared by repeatedly freezing and thawing the rinsed live cells (discussed above). Cytoplasm and water-soluble portions of cell walls were separated from insoluble cell walls of lysed cells by centrifugation and examined separately using ATR-FTIR spectroscopy.

**2.3. Diatom Cells.** Live diatom cells of *Thalassiosira weissflogii*, and their cleaned silica frustules (after removal of the outer organic layer), were examined using infrared spectroscopy. An axenic culture of this marine diatom (clone Actin, CCMP 1336) was obtained from the National Center for the Culture of Marine Phytoplankton (CCMP). The cultures were grown at 20 °C under a continuous saturating irradiance (provided by fluorescent bulbs below the cultures; flux density ~ 160 μmol m<sup>-2</sup> s<sup>-1</sup>). Cultures were maintained using natural seawater enriched with nutrients.<sup>43</sup> For collecting the infrared spectra of live diatoms, a centrifuged cell suspension was spread on the ATR crystal surface and progressively dried by gently blowing air on the wet sample paste. Infrared spectra of wet diatoms (initial wet paste) and air-dried diatoms were collected.

Cleaned diatom silica cell walls were prepared by initially collecting live cells on a polycarbonate filter with a 5 μm porosity and suspending them in 10% (w/v) sodium dodecyl sulfate (SDS) solution in deionized water. These samples were sonicated for three 15 s pulses in a Bransonic sonicator fitted with a microprobe tip (setting 6, 50% duty cycle), and centrifuged at 2500g for 10 min. The supernatant was discarded, and cell walls were resuspended, vortexed, and centrifuged as discussed above until the supernatant appeared colorless. A pelleted portion of this preparation was oxidized to remove surface glycoprotein by incubation in a 70% perchlorate solution at 70 °C for 2 h.

**2.4. Isolation of Cell Wall Fragments.** Bacteria were grown in TSB under an exponential growth phase as monitored by OD<sub>600</sub> measurements. Each culture was washed three times in 1 mM HEPES buffer, pH 6.8, and then passed through a French press operating at 20 000 psi to shear the cells. RNase, DNase (both from Sigma), and 1 mM MgCl<sub>2</sub> were added to the lysate to digest nucleic acids, and the large particulate fragments (cell envelopes) were removed by centrifugation at 150000g for 30 min. Gram-positive cell walls were boiled in 2% SDS to remove contaminating protein, and the residual SDS was removed by washing and centrifugation. The same procedure was used for the Gram-negative envelopes, and in this case, it removed the outer membrane, the periplasm, and contaminating proteins so that the peptidoglycan sacculi could be recovered. To avoid confusion, these Gram-negative peptidoglycan (or murein) sacculi are called Gram-negative cell wall fragments in this article.

**2.5. Infrared Spectroscopy Studies of Model Molecules and Cell Cultures.** ATR-FTIR spectra were obtained on a Bruker IFS66v/S (Billerica, MA) instrument using a narrow band mercury cadmium telluride (MCT) detector. Over 2000 scans with a 2 cm<sup>-1</sup> resolution were collected and averaged for each sample. The slit opening for the incident beam was set at 4 or 5 mm. Either AMTIR (refractive index = 2.5 and incident angle = 45° for bacterial and diatom suspensions at low pH and model molecules), Ge-60 (refractive index = 4.0 and incident angle = 60° for all cell suspensions, excepting *P. stutzeri*), or diamond (refractive index = 2.4 and incident angle = 60° for cell wall fragments and *P. stutzeri* cell suspensions) ATR crystals were used for collecting infrared spectra. Although the penetration depths are different for these different ATR crystals, the spectra of bacterial cells collected on different crystals were similar. However, a multireflection Ge-60 crystal was used for samples in the pH range of 4–10, and a single-reflection diamond crystal was used at all pH values when the sample volume was small. The ATR crystal surface was cleaned with water before running each sample, and the samples were spread carefully so as to cover the entire ATR crystal surface. Appropriate sample spectra

(43) Price, N. M.; Harrison, G. I.; Hering, J. G.; Hudson, R. J.; Nirel, P. M. V.; Palenik, B.; Morel, F. M. M. *Biol. Oceanogr.* **1988/89**, *6*, 443–461.

were used to remove spectral background, i.e., water for solution spectra of model compounds and supernatant of centrifuged cell suspensions for bacteria. Air was used as a background for Gram-negative cell wall fragments because the supernatant could not be easily centrifuged because their small sample size required high "g" forces. Back-titrations of model molecules and cells were performed to identify permanent chemical changes, if any, occurring during pH titrations. These studies indicated that the spectra of all model molecules were reproducible, but the cell suspensions showed minor variations when they were titrated to extreme pH values (pH <3.0 or >9.0).

### 3. Results and Discussion

The cell walls of bacteria consist of several polymers and macromolecules, which possess carboxyl, hydroxyl, phosphate, and amide functional groups.<sup>15,36</sup> Small model molecules containing one or more different functional groups with structural environments similar to those predicted for biomacromolecules in bacterial cell walls were chosen to evaluate vibrational bands of different functional groups. Infrared spectral variations of these model molecules as a function of pH were used to obtain information on the changes in vibrational states of different functional groups during protonation or deprotonation. Detailed spectral analyses of these model molecules were useful in identifying the functional groups of bacterial surfaces from their infrared spectra. It is likely that the coordination environments of these selected moieties in bacteria are different from those of the selected model molecules mainly because of variations due to H-bonding and substitution adjacent to the reactive functional groups. However, studies on model molecules can provide important information on the infrared absorption bands of different moieties in the bacterial cell and, as shown below, the infrared spectra of these model molecules and their variation as a function of pH resembled those of bacterial cells closely.

#### 3.1. Infrared Spectroscopy of Model Molecules.

**3.1.1. Alcohol Groups.** L-Rhamnose, a methyl pentose sugar commonly found in glycosides and in *P. aeruginosa* LPS, was used as a representative of molecules containing alcoholic hydroxyl groups. Although the infrared spectrum of aqueous rhamnose showed several absorption bands corresponding to C–O bonds in the range of 950–1200  $\text{cm}^{-1}$ , it was difficult to assign each peak to vibrations of a specific bond in the molecule (Figure 1). Identification of these bands was complicated by the strong vibrational coupling of C–O with the C–C and C–H bonds, which distributes its infrared absorption over several bands.<sup>55,63</sup> The hydroxyl groups in this molecule do not undergo deprotonation at pH values lower than 10, and their infrared spectra do not exhibit any spectral variations in this pH range (Figure 1).<sup>44</sup> The absence of spectral variations of hydroxyl group as a function of pH and vibrational coupling made their identification in bacteria difficult. As discussed later, the symmetric and asymmetric stretching vibrations of phosphate also absorb in this energy range, which complicated the unequivocal identification of both phosphate and hydroxyl groups. However, the vibrational bands of phosphate groups changed significantly with protonation and deprotonation in the pH range of 2–10.

**3.1.2. Carboxylic Acid Groups.** D-Glucuronic acid was used as a representative of organic molecules that contain both carboxylic acid and hydroxyl groups and is analogous to the teichuronic acids of Gram-positive walls (Figure 2). The structure of glucuronic acid is similar to that of

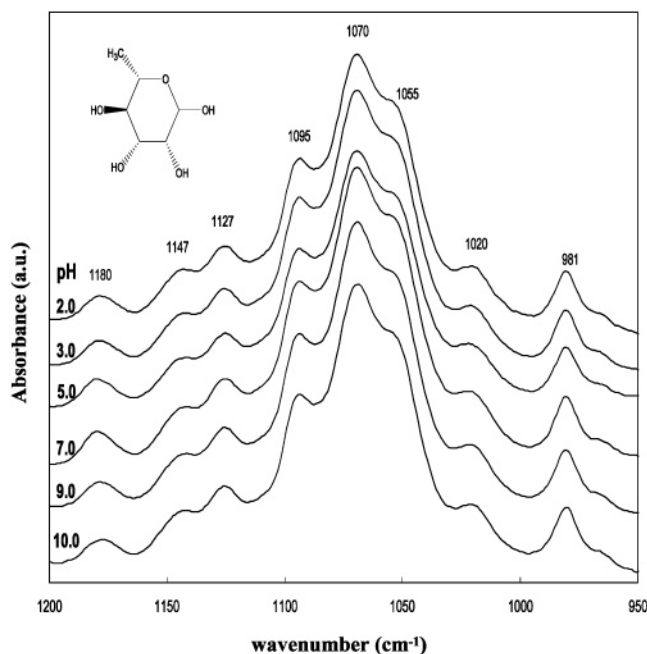


**Figure 1.** ATR-FTIR spectra of aqueous solution of L-rhamnose (50 mM) at pH 2.0, 3.0, 5.0, 7.0, 9.0, and 10.0 on AMTIR crystal. Approximate band positions are indicated in the figure. The inset shows the structure of the molecule.

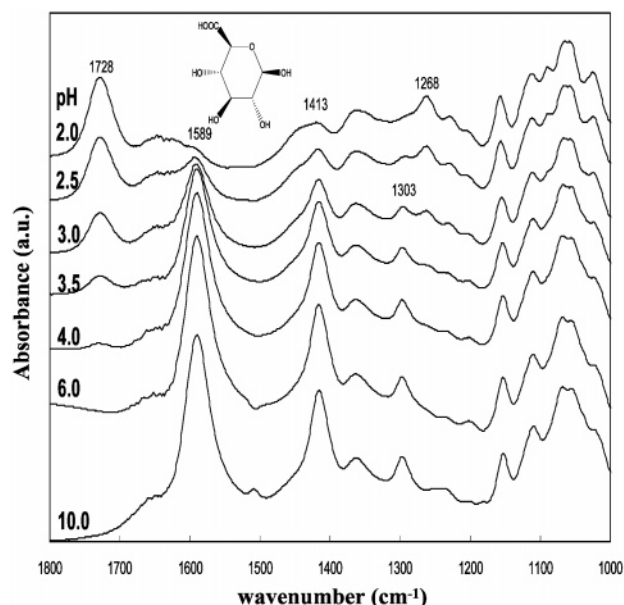


**Figure 2.** ATR-FTIR spectra of aqueous D-glucuronic acid (50 mM) at pH 2.0, 2.5, 3.0, 3.5, 4.0, 6.0, and 10.0 on AMTIR crystal. Approximate band positions are indicated in the figure. The inset shows the structure of the molecule.

rhamnose (discussed above), except for the addition of a carboxylic group in place of the methyl group in the former. Glucuronic acid exhibits spectral features that correspond to both carboxylic and alcoholic groups in the frequency ranges of 1200–1800 and 900–1200  $\text{cm}^{-1}$ , respectively (Figure 2). The C=O and C–OH of –COOH exhibited vibrational bands at 1728 and 1268  $\text{cm}^{-1}$ , respectively, in acid solutions. As the pH increased, the intensity of these bands decreased and new bands corresponding to the asymmetric and symmetric stretching of  $\text{COO}^-$  occurred at 1589 and 1413  $\text{cm}^{-1}$ , respectively (Figure 2).<sup>45,46</sup> On the

(44) Carey, F. A.; Sundberg, R. J. In *Advanced Organic Chemistry*; 3rd ed.; Plenum Press: New York, 1990; pp 179–255.

(45) Pouchert, C. J. *The Aldrich Library of FT-IR Spectra*, 2nd ed.; Aldrich: Milwaukee, WI, 1997.

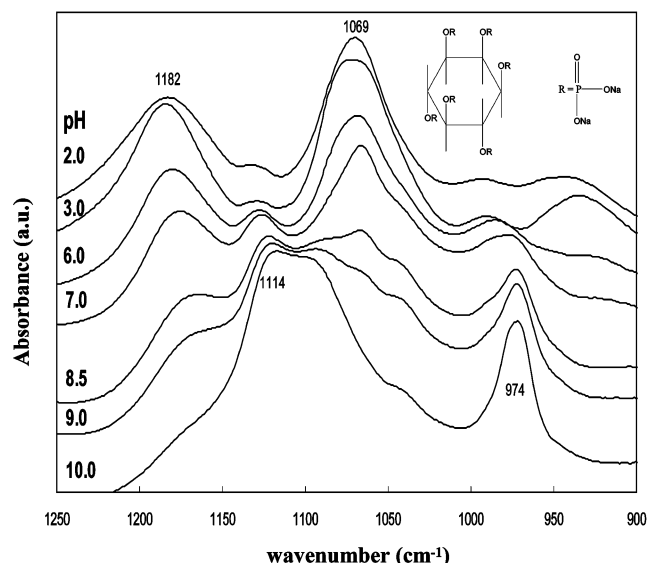


**Figure 3.** ATR-FTIR spectra of aqueous phytic acid (50 mM) at pH 2.0, 3.0, 6.0, 7.0, 8.5, 9.0, and 10.0 on AMTIR crystal. The inset shows the structure of the molecule.

basis of these spectral changes the  $pK_a$  (protonation or deprotonation constant) of the carboxylic acid group in glucuronic acid is expected to be between 3 and 4.<sup>42</sup>

In general, carboxylic acids exhibit similar spectral changes as they deprotonate and form carboxylate anions (see refs 46 and 47 and references therein). The asymmetric stretching vibrations of  $\text{COO}^-$  are also sensitive to the coordination environment of carboxylate anion, and these energies have been used to identify the type of carboxylate, such as aromatic and aliphatic, in bacterial walls.<sup>47,48</sup> In contrast, strong coupling of symmetric stretching vibration of carboxylate with the C–H, C–OH, and C–C groups makes it less sensitive to its structural environment.<sup>55,63</sup>

The spectral features of glucuronic acid in the energy range of 900–1200  $\text{cm}^{-1}$  were caused by the vibrations of C–OH (alcohol), C–C, and C–H groups, and these were similar to those seen with rhamnose, as discussed above. Small spectral variations in this energy range in acidic solutions may be due to intramolecular H-bonding between carboxylic and alcohol groups associated with carboxylic group deprotonation.

**3.1.3. Phosphate Groups.** Phosphate groups in bacteria can exist in several different forms: inorganic forms of phosphate such as orthophosphate and its oligomers, and organic species in the form of phosphate mono- and diesters. In this study, phytic acid (phosphate monoester) and tripolyphosphate were used as models to evaluate the behavior of phosphoryl groups in bacterial walls (Figure 3). Infrared spectroscopy of aqueous inorganic phosphates, conducted earlier by several investigators, indicates that the asymmetric and symmetric stretching vibrations of  $\text{PO}_4^{3-}$  are around 1010 and 935  $\text{cm}^{-1}$ , respectively (see ref 49 and references therein). Upon protonation, the asymmetric stretching of  $\text{PO}_{\text{unprotonated}}$  shifted to higher energies, with its absorption bands at 1077, 1155, and 1174  $\text{cm}^{-1}$  in the case of  $\text{HPO}_4^{2-}$ ,  $\text{H}_2\text{PO}_4^-$ , and  $\text{H}_3\text{PO}_4^0$ , respectively. Phosphate oligomers (pyro-

phosphate ( $\text{O}_3\text{P}-\text{O}-\text{PO}_3^{4-}$ ) and tripolyphosphate ( $\text{O}_3\text{P}-\text{O}-\text{PO}_3-\text{PO}_3^{5-}$ ) also exhibited features similar to those of protonated phosphates. The asymmetric stretching modes of the  $\text{PO}_{\text{unprotonated}}$  groups of these species were in the range of 1160–1240  $\text{cm}^{-1}$ , with the highest value being for the protonated tripolyphosphate. With deprotonation of protonated tripolyphosphate, the band around 1240  $\text{cm}^{-1}$  decreased in intensity and gradually shifted to a lower energy (1199  $\text{cm}^{-1}$ ), indicating that the P=O character weakened (similar to orthophosphate, discussed above). Although protonated phosphate groups (P–OH, and also the P–O–P vibrations in the case of phosphate oligomers) are also sensitive to protonation, these bands occurred in the energy range of 850–1010  $\text{cm}^{-1}$  and overlapped with the carbohydrate features, discussed above. This made their identification ambiguous.

The linking of a phosphate group to an organic molecule, such as in phosphate mono- and diesters, also modifies phosphate group vibrations, and these changes are similar to those found in protonated and polymerized phosphates. Phytic acid consists of six phosphate groups, each connected to a six-membered aliphatic carbon ring through one of the oxygen atoms of phosphate, and the  $pK_a$  values of these phosphates range from 1.9 to 9.5.<sup>50</sup> Around pH 2.0 (above the lowest  $pK_a$  of phytic acid), aqueous phytic acid exhibited an intense peak corresponding to the  $\text{PO}_{\text{uncomplexed}}$  at 1182  $\text{cm}^{-1}$ . With an increase in pH, its intensity decreased and new peaks appeared at 1114 and 974  $\text{cm}^{-1}$ , which correspond to the asymmetric and symmetric stretching vibrations of deprotonated phosphoryl groups ( $\text{PO}_3$  and  $\text{PO}_2$ ), respectively.<sup>51</sup> These spectral changes were caused by the gradual deprotonation of the multiprotic phosphate groups in this molecule with the increase in pH. Similarly, the asymmetric stretching vibrations of  $\text{PO}_{\text{uncomplexed}}$  in phosphate diesters have been shown to absorb strongly around 1240  $\text{cm}^{-1}$ .<sup>52</sup> In addition, H-bonding interactions of the  $\text{PO}_{\text{uncomplexed}}$  groups may weaken the P=O bond character and shift its absorption bands to lower energy. Similar spectral changes are observed in the case of tris(2-ethylhexyl) phosphate.<sup>53</sup> Infrared spectroscopy of inorganic and organophosphates suggest that pH-dependent spectral variations around 1200  $\text{cm}^{-1}$  can be attributed to phosphate groups. However, distinguishing the inorganic and organic phosphates may be difficult.

A summary of infrared spectral changes of model molecules indicates that the carboxylic and phosphate groups exhibit dominant changes around 1720 and 1200  $\text{cm}^{-1}$ , respectively, with changes in pH. The hydroxyl, C–H, and C–C groups of carbohydrates exhibited several bands in the energy range of 900–1200  $\text{cm}^{-1}$ , but did not exhibit significant changes with pH. Although the amide groups are common in the protein backbone, their models were not examined here. However, previous infrared and Raman spectroscopic studies of molecules containing amides indicated that the C=O of amide (referred to as amide I) and N–H bending (coupled to C–N and referred to as amide II) occur in the range of 1600–1700 and 1520–1550  $\text{cm}^{-1}$ , respectively.<sup>45,54,55</sup> The amide II band is noticed

(50) Birrell, H. C.; Camilleri, P.; Okafo, G. N. *Chem. Soc., Chem. Commun.* **1994**, 1, 43–44.

(51) Bartl, F.; Úrjasz, H.; Brzezinski, B. *J. Mol. Struct.* **1998**, 441, 77–81.

(52) Wong, P. T. T.; Papavassiliou, E. D.; Rigas, B. *Appl. Spectrosc.* **1991**, 45, 1563–1567.

(53) Brzezinski, B.; Bartl, F.; Zundek, G. *J. Phys. Chem. B* **1997**, 101, 5607–5610.

(54) Pavia, D. L.; Lampman, G. M.; Kriz, G. S. *Infrared Spectroscopy. In Introduction to Spectroscopy*; Daunders College Publishing: Orlando, FL, 1996; pp 14–29.

(46) Strathmann, T. J.; Myneni, S. C. B. *Geochim. Cosmochim. Acta* **2004**, 68, 3441–3458.

(47) Hay, M. B.; Myneni, S. C. B. To be submitted for publication.

(48) Leenheer, J. A.; Wershaw, R. L.; Reddy, M. M. *Environ. Sci. Technol.* **1995**, 29, 393–398.

(49) Persson, P.; Nilsson, N.; Sjöberg, S. *J. Colloid. Interface Sci.* **1996**, 177, 263–275.

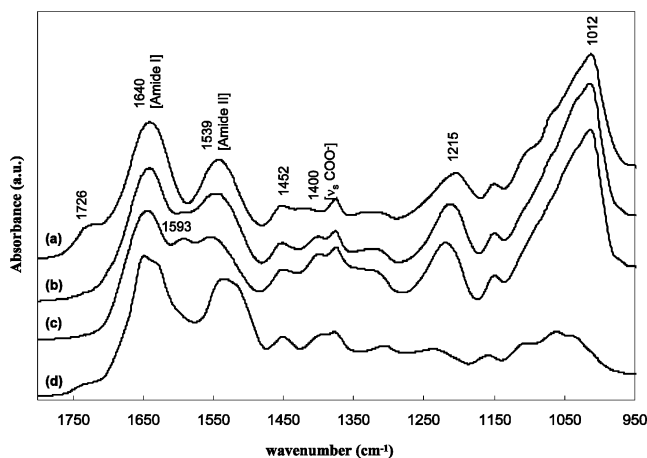


**Figure 4.** ATR-FTIR spectra of cell walls of *B. subtilis* (a–c) and *P. aeruginosa* (d; pH  $\sim$ 6.0) on diamond crystal. (a), (b), and (c) correspond to samples at pH values of 2.0, 4.0, and 6.0, respectively. Approximate band positions are indicated in the figure.

only in primary and secondary amides (because of the N–H contribution). Previous studies also indicate that the energies and intensities of amide I and II bands are sensitive to the conformational changes of the protein. The energy and spectral variation of these characteristic bands corresponding to different functional groups were used to identify these groups in cell walls of bacteria.

### 3.2. Infrared Spectroscopy of Cell Wall Fragments.

Isolated cell wall fragments of both Gram-positive and Gram-negative cells were examined using ATR-FTIR spectroscopy (Figure 4). The isolated walls of *B. subtilis* examined in this study were composed of peptidoglycan and teichoic acid, and those of *P. aeruginosa* contained peptidoglycan only. Although the infrared spectra of these cell wall fragments and intact bacterial cells exhibit similar bands, differences existed between the walls of *B. subtilis* and *P. aeruginosa* (Figures 4 and 5). The wall fragments exhibited distinct bands around 1640 and 1540  $\text{cm}^{-1}$  corresponding to amide,  $\sim$ 1215  $\text{cm}^{-1}$  corresponding to phosphate, and in the range of 950–1100  $\text{cm}^{-1}$  corresponding to carbohydrates. On the basis of the energies of the amide I and amide II bands, they were considered as primary or secondary amides or a mixture of both. Carboxylate vibrations were not distinct in the infrared spectra of the wall fragments because of the near-neutral pH of the wall suspensions (pH  $\sim$ 6.0). However, the presence of carboxylates in the fragments was clearer when the sample pH was lowered to 2.0 (details discussed below). The *B. subtilis* walls exhibited stronger bands corresponding to carbohydrate and phosphate groups because of the presence of teichoic acids in them.

Variations in the infrared spectra of cell wall fragments of *B. subtilis* were revealed as the pH was varied from 2.0 to 6.0 (pH of cell culture), to 10.0 (Figure 4). The spectral changes were distinct for carboxyls and amides. The C=O of carboxylic acid exhibits a peak at 1726  $\text{cm}^{-1}$ . The intensity of this peak decreased, and the asymmetric and symmetric stretching of deprotonated  $\text{COO}^-$  groups appeared at 1593 and 1400  $\text{cm}^{-1}$ , respectively, with an increase in pH. The presence of the asymmetric stretching of the carboxylate band at this energy indicated that the carboxylate groups were adjacent to other groups, such as an  $\alpha$ -OH.<sup>47</sup> Although the appearance of this new band

alters the energy, width, and intensity of the amide bands, the contributions to spectral variations from changes in protein conformations cannot be ruled out. Minor spectral variations were also found for the phosphate band around 1215  $\text{cm}^{-1}$  and for the carbohydrate bands in the range of 1050–1110  $\text{cm}^{-1}$ . However, it is difficult to attribute these variations to a particular functional group because of the significant overlap of several bands in this energy region.

### 3.3. Infrared Spectroscopy of Cell Suspensions.

**3.3.1. Sensitivity Test of ATR-FTIR to Bacteria Surfaces.** Live diatom cells with a thin glycoprotein layer over the silica shell and FTIR spectra of lysed and intact cells were used as model systems for estimating the penetration depth of the evanescent wave at the interface of the ATR crystal.

The thickness of the external glycoprotein layer is about 8–10 nm in the examined diatoms.<sup>56</sup> The diatoms cleaned with perchlorate do not have this organic layer, and their infrared spectrum showed two bands at  $\sim$ 1630 (weak) and 1100 (strong)  $\text{cm}^{-1}$  corresponding to water bending and Si–O stretching vibrations, respectively (Figure 6). In contrast, the live diatoms showed several strong peaks in the energy range of 1150–1800  $\text{cm}^{-1}$ , which are similar to those found in the isolated bacterial cell walls, discussed above. The absence of a strong 1100  $\text{cm}^{-1}$  band and the presence of all other bands representative of organic molecule functional groups from the live diatom samples are noteworthy. With progressive drying of the live suspension on the ATR crystal surface, the infrared absorption between 1100 and 1200  $\text{cm}^{-1}$  increased. In addition, the amide I band at 1640  $\text{cm}^{-1}$  shifted to a lower energy and the amide II band at 1540  $\text{cm}^{-1}$  decreased in intensity.

These infrared spectra of diatoms, with and without the thin glycoprotein layer, indicated that the collected ATR-FTIR spectra could distinguish between the two diatom surfaces even though the glycoprotein layer was only a few nanometers thick. Clearly the infrared signal could penetrate at least to this thickness. Although the estimated penetration depth for the ATR crystal with the highest refractive index and highest angle of incidence (Ge-60) is greater than 190 nm ( $<$ 1800  $\text{cm}^{-1}$ ), the actual penetration into the sample appears to be much smaller. Such a shallow penetration may be caused by several factors: (a) the presence of a water film several tens of nanometers thick between the ATR crystal and the diatoms, (b) an open and expanded structure of glycoprotein in water when compared to the conditions under which the organic film thickness was measured (e.g., vacuum in electron microscopes), and (c) a progressive increase in the refractive indices of diatom surfaces as the evanescent wave penetrates from water into the organic film and silica frustule, which may alter the wave propagation significantly and mean that the penetration depth estimates from eqs 1 and 2 are not valid. The observed changes in band intensities in the 1100–1200  $\text{cm}^{-1}$  region with sample drying may be caused by the diatom cells approaching closer to the ATR crystal and an increase in the concentration of cells that are in direct contact with the ATR crystal. During dehydration, the glycoprotein layer presumably changed from an open to condensed molecular structure, and this would also modify band intensity.

ATR-FTIR spectra of lysed and intact cells were also compared to identify the sensitivity of this technique to

(55) Edwards, D. C.; Nielsen, S. B.; Jarzecki, A. A.; Spiro, T. G.; Myneni, S. C. B. Submitted for publication in *Geochim. Cosmochim. Acta* 2004.

(56) Volcani, B. E. In *Biochemistry of Silicon and Related Problems*; Bendz, G., Lindqvist, I., Ed.; Plenum Press: New York, 1978; pp 177–204.

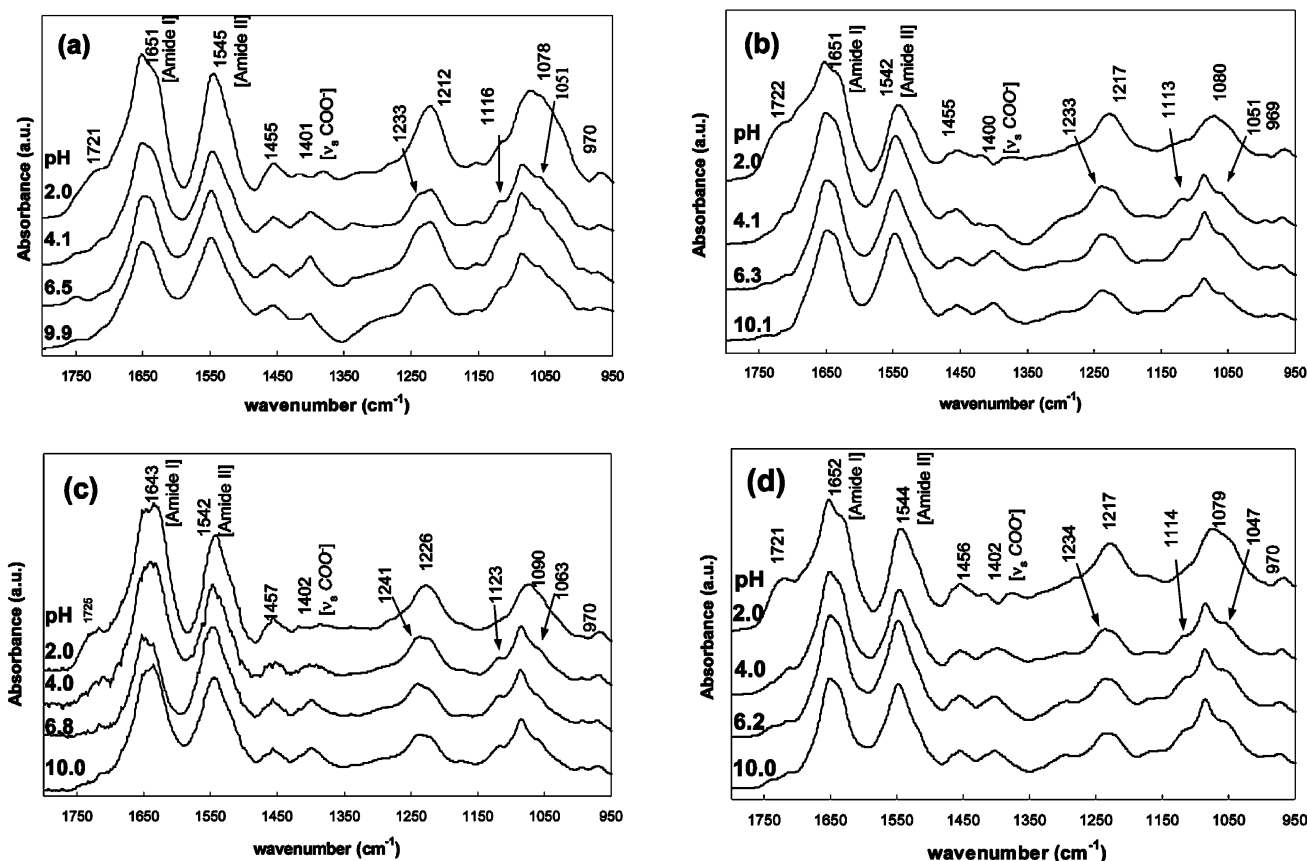


**Figure 5.** ATR-FTIR spectra of intact Gram-positive (a, b) and Gram-negative (c, d) cells on Ge-60 crystal. (a) *B. subtilis*, (b) *B. licheniformis*, (c) *P. stutzeri*, and (d) *P. aeruginosa*. Each frame shows four spectra, collected for cells at different pH values (indicated in the figure). Approximate band positions are indicated in the figure.

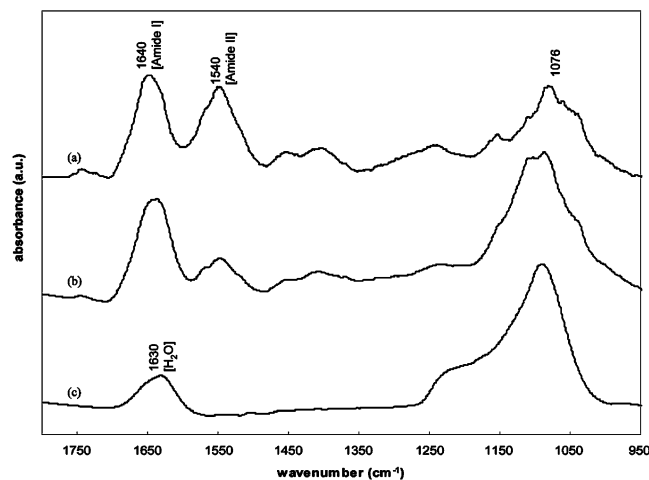


**Figure 6.** ATR-FTIR spectra of (a) wet live diatom, (b) air-dried live diatom, and (c) cleaned diatom on AMTIR crystal. Approximate band positions are indicated in the figure.

bacterial surfaces (Figure 7). These studies indicate that the amide II and carbohydrate bands (around 1520 and 1080 cm<sup>-1</sup>, respectively) of soluble cytoplasm-rich fluid of the cell interior are different from those of the intact cells. In addition, the ATR-FTIR spectra exhibited different spectral variations for intact and lysed cells as a function of pH. These studies suggest that the ATR-FTIR spectroscopic results presented above for the intact cells may represent the surface macromolecular composition.

Although these ATR-FTIR measurements did not provide an absolute penetration depth, they did indicate

that the ATR spectra of aqueous cell suspensions are highly sensitive to surfaces. It is reasonable to assume that the optical properties (e.g., refractive index) of the bacterial surface and those of the organic layer on the diatom cell surface are very similar. Hence, it is understood that the ATR-FTIR spectra of the bacteria presented below mostly reflect the properties of the bacterial cell wall and not the interior of the cell. As discussed later, the similarities in the infrared spectra of cell wall fragments and the intact cells also lend support to this hypothesis.

**3.3.2. Functional Group Chemistry of Bacteria Surfaces.** The infrared spectra of Gram-positive (*B. subtilis* and *B. licheniformis*) and Gram-negative (*P. stutzeri* and *P. aeruginosa*) bacteria in aqueous solution as a function of pH and growth stage were examined using ATR-FTIR spectroscopy (Figure 5). Their infrared spectra exhibited distinct peaks corresponding to carboxyls, amides, phosphates, and carbohydrates (Figure 5, Tables 1 and 2). Some of the bacterial species were also grown at least three times to evaluate variations in their infrared spectra, and these studies indicated that the energy and relative intensities of vibrational bands were highly reproducible (energy variation < 2 cm<sup>-1</sup>). Interestingly, the infrared spectra of both Gram-positive and Gram-negative bacteria were similar and exhibited similar variations as a function of changes in pH. The similarity is presumably because the Gram-negative walls consisted of only peptidoglycan sacculi and peptidoglycan is a major component of the Gram-positive cell walls. The maximum spectral changes observed were in the pH range of 2–4, and changes above this pH range were minor.

**Carboxyl Groups.** The carboxylic groups of bacterial cells exhibited a distinct band at ~1720 cm<sup>-1</sup> corresponding to

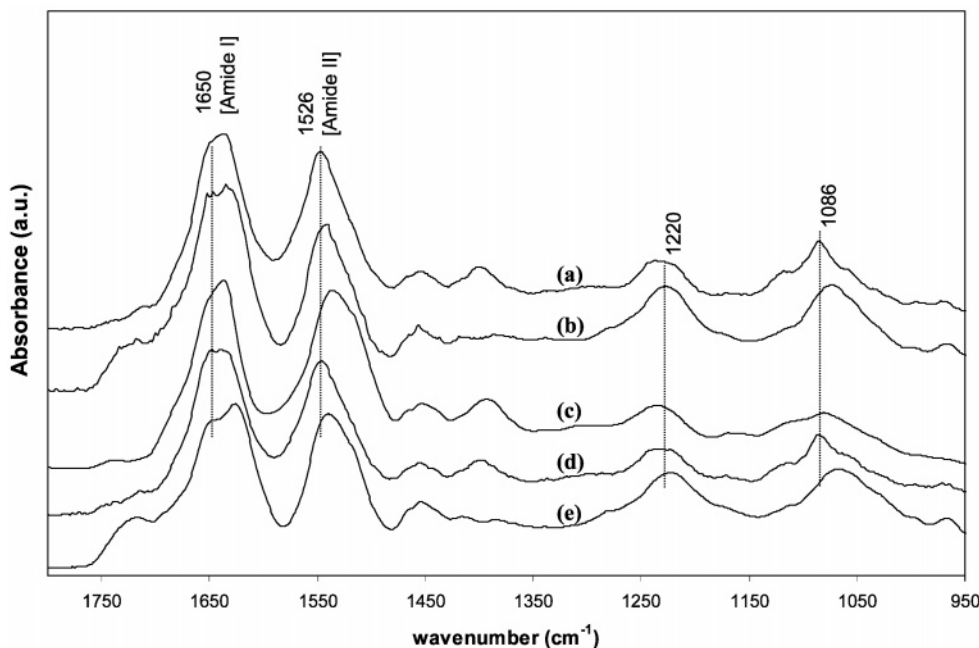


**Figure 7.** ATR-FTIR spectra of intact *P. stutzeri* cells at pH 6.0 (a) and 2.0 (b), and their lysed cells (c–e). (c) Soluble fraction of lysed cells, (d) soluble fraction and cell walls, and (e) same as (d) but at pH 2.0. Approximate band positions are indicated in the figure.

**Table 1. Absorption Bands of Bacterial Surface Functional Groups<sup>a</sup>**

abs bands (cm <sup>-1</sup> )	vibrational modes
1721	stretching of C=O in protonated carboxylic acid group
1646	stretching of C=O in amide (amide I)
1541	N–H bending and C–N stretching in amide (amide II)
1450	CH <sub>2</sub> scissoring
1396	symmetric stretching of COO <sup>-</sup>
1233	vibrations of –COOH, and C–O–C group in esters
1211	stretching of P=O bond in phosphate
950–1150	asymmetric and symmetric stretching of PO <sub>2</sub> <sup>-</sup> and P(OH) <sub>2</sub> in phosphate; vibrations of C–OH and C–C bonds in polysaccharides and alcohols

<sup>a</sup> Several of the bands identified are broad, and the band position represents the center of the band maximum.

the C=O in acidic cell suspension (pH ≤ 4.0). The intensity of this peak decreased as the sample pH increased, and this spectral change was similar to that of glucuronic acid, discussed above. Although the asymmetric stretching vibrations of the deprotonated carboxylate anion, COO<sup>-</sup>, was expected to appear around 1590 cm<sup>-1</sup> in alkaline cell suspensions (pH ≥ 4.0), it was obscured by the intense amide bands in the range of 1500–1650 cm<sup>-1</sup>. However, the symmetric stretching of COO<sup>-</sup> vibration appeared around 1396 cm<sup>-1</sup>, which was absent in all samples previously examined at acidic pH. The C=O of protonated carboxylate band around 1720 cm<sup>-1</sup> was almost absent or extremely weak in alkaline cell suspensions. This suggests that (i) ATR-FTIR studies are surface sensitive (similar to the diatom surfaces) and the majority of the carboxylate groups probed using this method were on the bacterial wall surfaces, and/or (ii) the protons can diffuse rapidly inside the cell wall and protonate the carboxylates present inside the plasma membrane and the cytoplasm.

**Amide Groups.** The amide groups exhibited intense bands around 1650 and 1550 cm<sup>-1</sup> corresponding to the amide I and amide II bands, respectively. Although variations in the energies and intensities of these bands were minor with changes in pH, the intensity ratio of amide I to amide II decreased with an increase in pH. These minor variations in the infrared spectra of amide

groups may be caused by (i) appearance of new peaks in this energy region (e.g., corresponding to COO<sup>-</sup>), which may modify the intensity and energy of amide bands (similar to the variations observed in the case of isolated cell wall fragments), and (ii) changes in protein conformations. Although the insensitivity of amide vibrations to pH fluctuations may suggest that a majority of amide groups are inside the cell wall, this seems unlikely. This is because the isolated cell wall fragments showed intense bands corresponding to amides, and their spectral variations with pH, even if they are minor, were similar to those reported for intact cells (Figures 4 and 5).

The spectral intensity of carboxylate and amide groups can give information on the relative concentration of these groups. A comparison of their intensity ratio with those of known molecules can provide information on the relative concentration of these groups in the cell wall. For example, the infrared spectrum of aqueous Lisinopril, which contains an amide and two carboxylic acid groups, exhibits an intensity ratio of 1.61 for amide I and C=O of a protonated carboxyl.<sup>57</sup> The solid spectra of several compounds that contain amides and carboxyls exhibit a ratio that ranges from 1 to 1.1 (average from 1-(aminocarbonyl)-1-cyclopropanecarboxylic acid, *N*-acetylneuraminic acid, 1-acetyl-4-piperidinecarboxylic acid, succinic 2,2-dimethylhydrazide, *N*-(*tert*-butoxycarbonyl)-L-serine, and D-alanyl-glycine).<sup>58</sup> However, the aqueous spectrum of Lisinopril may represent the bacteria sample better than these other solid samples because of its sample state. When the ratio of amides to carboxylic groups are estimated using this ratio from Lisinopril and the measured spectral intensity of carboxylates and amides in bacterial suspensions at pH 2.0, the concentration ratio of amide to carboxylic groups is in the range of 1.5–2.5 (2.5–4.0 when solid references used). Variations in this ratio may be partly attributed to improper subtraction of spectral background from water (water bending vibrations are around 1630

(57) Wang, S. Chuang, C.; Lin, S. *Chem. Pharm. Bull.* **2002**, *50*, 78–82.

(58) Pouchert, C. J. *The Aldrich Library of FT-IR Spectra*, 2nd ed.; Aldrich, Milwaukee, WI, 1997.

**Table 2. Absorption Bands of the Dominant Surface Functional Groups of Different Bacterial Species and Their Cell Walls at pH ~6.0**

functional group	<i>B. subtilis</i>	<i>B. licheniformis</i>	<i>P. stutzeri</i>	<i>P. aeruginosa</i>	cell wall of <i>B. subtilis</i>	cell wall of <i>P. aeruginosa</i>
amide I	1651	1651	1643	1652	1640	1647
amide II	1545	1542	1542	1544	1539	1535
CH <sub>2</sub> scissoring	1455	1455	1457	1456	1452	1452
$\nu_s$ COO <sup>-</sup>	1401	1400	1402	1402	1400	1397
COOH, P=O	~1230	~1230	~1240	~1230	~1220	~1240 <sup>a</sup>
-P(OH) <sub>2</sub> , -C-OH	~1100	~1100	~1100	~1100	~1012	~1050

<sup>a</sup> Weak.

cm<sup>-1</sup>). When this ratio is compared with the ratio of carboxyl to amide in structurally well-characterized biomacromolecules, it is around 1:5 and 1:3 for peptidoglycon in Gram-positive and Gram-negative cells, respectively. Although several major constituents of cell walls are not well characterized to make an accurate estimate of this ratio, this ratio obtained from infrared spectra may represent the average ratio of carboxyls and amides present in bacterial surface membranes.

**Phosphate Groups.** As discussed earlier, it is difficult to identify different phosphate groups unambiguously from the infrared spectra alone. On the basis of the spectral variations reported for different types of phosphates, the absorption band around 1210 cm<sup>-1</sup> was assigned to the stretching of the P=O bonds of phosphate diester or protonated polyphosphate (details discussed above). The relative intensity of this peak also decreased at pH values 4 and above, which is consistent with the trends seen in the case of organophosphates (Figure 3). Although the C-OH bonds of carboxylic acids absorb in the same energy region, the spectral variation around 1210 cm<sup>-1</sup> is too low to be attributed to C-OH groups. In addition, spectral variations in this region were also accompanied by variations around 1100 cm<sup>-1</sup>, where the P-OH bands vibrate (discussed later). Another strong band around 1233 cm<sup>-1</sup>, which was not affected by pH variations, may have been caused by functional groups, such as esters (C-O-C vibrations) and phosphate groups inside the cell wall.

The infrared spectra of intact Gram-positive and Gram-negative cells are identical in the spectral region corresponding to phosphate groups while their isolated cell wall fragments are significantly different (Figures 4 and 5). It should be noted that the isolated cell wall fragments of Gram-positive cells contain both peptidoglycan and teichoic acids, and the Gram-negative cells contain peptidoglycan only. Since the outer membranes of intact Gram-negative cells contain phospholipids, which have phosphate groups in the same local coordination environment as phosphate in teichoic acids, the sum spectra of peptidoglycan + teichoic acids of Gram-positive cells, and peptidoglycan + outer membrane of Gram-negative cells, are expected to be similar.

**Polysaccharide and Related Groups.** The C-OH (alcohol), C-C, and some of the C-H vibrations exhibited a broad band in the energy region of 950–1150 cm<sup>-1</sup>. With an increase in pH, the band at 1080 cm<sup>-1</sup> became sharp along with sharpening of a weak band around 1115 cm<sup>-1</sup> and weakening of the high-energy shoulder around 1050 cm<sup>-1</sup>. These changes were at a maximum between pH 2.0 and 4.0, and may be caused by variations in the H-bonding interactions associated with the deprotonation of carboxylate groups and the variations in the protonation state of phosphate groups. These changes were consistent in all of the Gram-positive and Gram-negative species examined in this study.

A strong band at 1450 cm<sup>-1</sup> was insensitive to pH variation, and this is characteristic of the scissoring motion of CH<sub>2</sub> groups,<sup>45</sup> which are common in peptidoglycan,

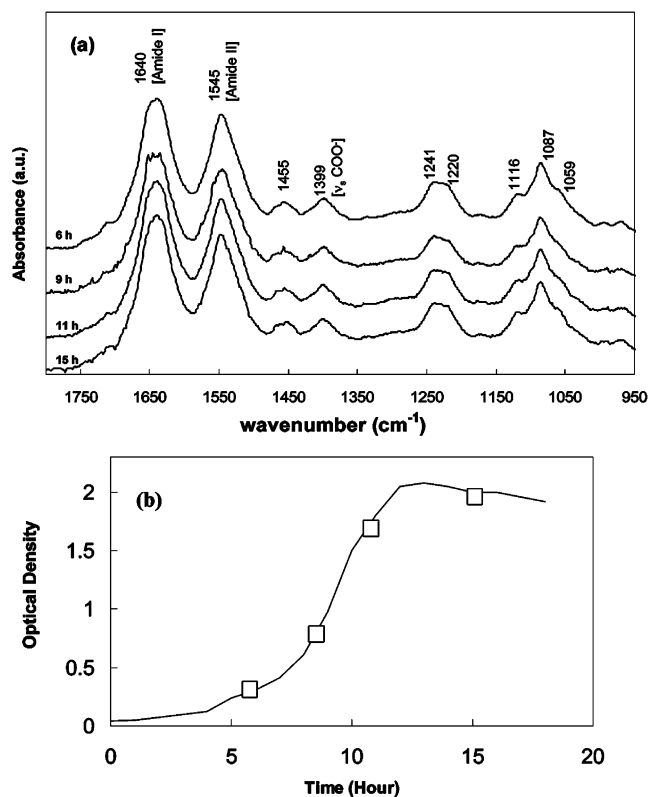


**Figure 8.** Surface chemistry of bacteria as a function of growth phase. (a) ATR-FTIR spectra of *P. stutzeri* in different growth phases. (b) Growth curve for *P. stutzeri*. Small boxes in (b) represent sampling times for ATR-FTIR spectroscopy studies. Approximate band positions are indicated in the figure.

teichoic acid, LPS, and phospholipids. Kamnev et al. also observed similar peaks in IR spectra of isolated bacterial membranes.<sup>36</sup>

**3.3.3. Influence of Growth Phase and Growth Medium on Cell Surface Chemistry.** Previous research has shown that metabolically active cells, live nonmetabolically active (or resting) cells, and dead cells possess cell walls of different surface reactivities, possibly due to competition with protons generated by the cell's energized membrane or because of changes in surface functional groups.<sup>37,38</sup> To determine whether the functional group chemistry of the bacterial cell surface changes as a function of its growth stage, IR spectra of *P. stutzeri* were obtained at different growth stages of the organism (Figure 8). These cells at different growth stages showed similar infrared spectral features without significant changes in the energy and intensity of bands. This implies that the dominant functional groups on bacterial cell walls do not change over time with growth.

The influence of growth medium on the surface chemistry of microorganisms was also examined (Figure 9). Infrared spectra of *P. stutzeri* grown in LB and TSB were identical, indicating that differences in these nutrient-

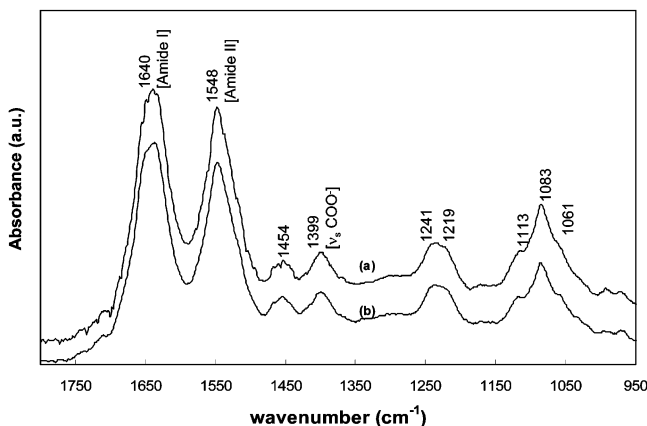


**Figure 9.** Influence of growth medium on bacteria cell surface chemistry. ATR-FTIR spectra of *P. stutzeri* grown in (a) TSB medium and (b) LB-broth medium under the same growing conditions. Approximate band positions are indicated in the figure.

rich growth media do not alter the dominant functional groups on bacterial surfaces.

#### 4. Summary and Conclusions

This in situ ATR-FTIR study demonstrates the advantages and limitations of infrared spectroscopy in distinguishing different functional groups on bacteria surfaces. Although the ATR-FTIR spectroscopy technique is surface sensitive, the sensitivity of this technique to distinguishing different cell surface membranes cannot be established directly. However, the ATR-FTIR measurements on intact and lysed cells and live and clean diatoms suggest that this technique provides surface-sensitive information.

Results presented in this study also showed that the dominant functional groups of bacterial surfaces are carboxyl, amide, phosphate, hydroxyl, and carbohydrate related moieties. Contrary to the general understanding that Gram-positive bacterial cell walls exhibit significant differences from Gram-negative cell walls in both structure and chemical composition, infrared spectroscopic results presented here suggest that the bulk functional group chemistry of both classes of bacterial surfaces are identical. These findings are in line with the identical macroscale sorption behavior of different metals onto Gram-positive and Gram-negative bacteria and their mixtures.<sup>59</sup> Although these infrared spectroscopic results indicate the universality of the functional group chemistry of bacteria

(59) Yee, N.; Fein, J. B. *Geomicrobiol. J.* **2003**, *20*, 43–60.

cell surfaces, differences between them may exist for the minor components and their structure. These differences may lead to variations in reactivity when subjected to straining techniques used in distinguishing the Gram-positive and Gram-negative bacteria, and further in-depth studies are necessary to identify the structural differences in functional groups between them.

Among different functional groups, we find that carboxylic, phosphate, and carbohydrate groups are sensitive to changes in solution pH, and the deprotonation of the first two may lead to the net negative surface charge of bacteria surfaces in the ambient pH range of 4–9. Previous potentiometric titrations have also identified them as the primary sites that can deprotonate in the acidic pH range.<sup>23,24,60</sup> While a majority of carboxylic acid groups have  $pK_a$  values below 5.0, the phosphate groups have a wide range of  $pK_a$  values, which decrease with phosphate polymerization (e.g., from phosphoric acid to triphosphoric acid<sup>61</sup>). The phosphate mono- and diesters common in bacterial cell walls also exhibit strong acidic behavior. Because of their sensitivity in the acidic pH range, both carboxylic and phosphate groups can act as metal binding sites below a pH of 5.0.<sup>62</sup> The absence of changes in amide groups with pH may suggest that the macromolecular structure of the protein backbone may not change significantly with solution pH.

ATR-FTIR spectroscopic results presented here demonstrate that bacterial surface chemistry does not change significantly with either the growth phase or the nutrient-rich growth media. Although nutrient-rich growth media commonly used by microbiologists are tested in this investigation, it will be important to test the influence of extreme concentration of metals and organic molecules on the cell wall chemistry. This information will be useful in identifying the behavior of bacteria in nature.

**Acknowledgment.** The authors thank Dr. A. Milligan for providing diatom samples, and Dr. A. Deshmukh for reviewing the manuscript. This work was supported by a NSF (Chemical Sciences) grant to S.C.B.M. and a NSERC-discovery grant to T.J.B.

LA049043+

(60) Daughney, C. J.; Fein, J. B.; Yee, N. *Chem. Geol.* **1998**, *144*, 161–176.

(61) Kerst, A. F. *Environmental Phosphorous Handbook*; Griffith, E. J., Beeton, A., Spencer, J. M., Mitchell, D. T., Eds.; John Wiley & Sons: New York, 1973; p 267.

(62) Boyanov, M. I.; Kelly, S. D.; Kemner, K. M.; Bunker, B. A.; Fein, J. B.; Fowle, D. A. *Geochim. Cosmochim. Acta* **2003**, *67*, 3299–3311.

(63) Quilès, F.; Burneau, A.; Gross, N. *Appl. Spectrosc.* **1999**, *53*, 1061–1070.